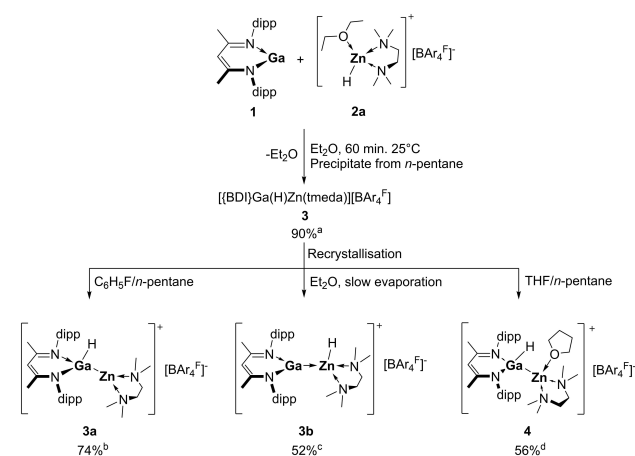


heterobimetallics derived from **1** and Lewis-acidic zinc hydride cations $[\text{L}_n\text{ZnH}]^+$.^[19]

Adding an equimolar quantity of $[(\text{BDI})\text{Ga}]$ (**1**) to a Et_2O solution of $[(\text{tmeda})\text{ZnH}(\text{OEt}_2)][\text{BAR}_4^{\text{F}}]$ (**2a**; $\text{BAR}_4^{\text{F}} = [\text{B}(3,5\text{-}(\text{CF}_3)_2\text{-C}_6\text{H}_3)_4]^-$)^[19] provided compound **3**, which was isolated in 90% yield as beige microcrystals by precipitation into *n*-pentane (Scheme 2). Recrystallisation from fluoro-benzene/*n*-pentane provided colourless X-ray quality single crystals of the charge-separated ion pair $[(\text{BDI})\text{Ga}(\text{H})\text{-Zn}(\text{tmeda})][\text{BAR}_4^{\text{F}}]$ (**3a**) in the monoclinic space group $P2_1/n$. The two metals are connected by an unsupported bond, the length of which (2.3973(11) Å) is typical of a covalent bond between these elements.^[20] The three-coordinate TMEDA-ligated zinc centre lies in an approximately trigonal planar environment (Figure 1), whilst the four-coordinate gallium



Scheme 2. Synthesis of compound **3** and crystallisation of **3a**, **3b**, and **4**. ^a Isolated yield of product precipitated from $\text{Et}_2\text{O}/n\text{-pentane}$.

^b Isolated yield of product recrystallised from $\text{C}_6\text{H}_5\text{F}/n\text{-pentane}$; crystallises as gallium hydride isomer **3a** with 6% co-crystallised isomer **3b**.

^c Isolated yield of product after recrystallisation by slow evaporation of a Et_2O solution; crystallises as zinc hydride isomer **3b** with trace co-crystalline **3a**. ^d Isolated yield of product recrystallised from $\text{THF}/n\text{-pentane}$; crystallises as THF-adduct **4**.

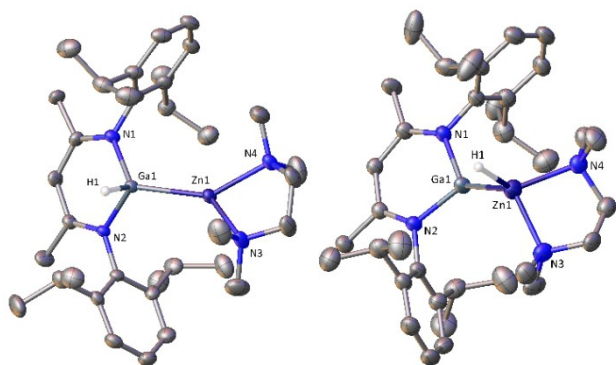


Figure 1. Structures of the cationic parts of **3a** (left) and **3b** (right) in the crystal. For clarity, hydrogen atoms are omitted except for the hydride ligand, and thermal ellipsoids are shown at the 50% level. Only the major part of the disordered TMEDA ligand in **3b** is shown. The minor component of the disordered bimetallic core in **3a** is omitted.

centre adopts a distorted tetrahedral geometry. The terminal gallium-bound hydride ligand was unambiguously located in the Fourier difference map and freely refined. Significant residual electron density located near the metal centres was attributed to a minor co-crystallised component (6% occupancy) of isomeric $[(\text{BDI})\text{Ga}\rightarrow\text{Zn}(\text{H})(\text{tmeda})][\text{BAR}_4^{\text{F}}]$ (**3b**), consistent with the solution-state isomerisation behaviour observed by ^1H NMR spectroscopy (see below).

The zinc-hydride isomer **3b** could be crystallised as the major component by slow evaporation of a concentrated Et_2O solution of **3**. The crystal structure was solved in the triclinic space group, $P\bar{1}$, and contains a separated ion pair with two molecules of Et_2O per asymmetric unit. Residual electron density near both metal centres possibly results from traces of co-crystallised **3a**. A zinc-bound hydride was located and freely refined, and its location is further supported by other structural features. Namely, the gallium centre adopts a near planar trigonal geometry ($\Sigma = 357^\circ$) and is connected to the zinc atom via a bond of 2.4766(16) Å in length. This distance is almost 0.08 Å longer than that of **3a**, but similar to previously reported $\text{Ga}^{\text{I}}\rightarrow\text{Zn}^{\text{II}}$ donor-acceptor complexes,^[20f,21] and thus consistent with a dative $\text{Ga}\rightarrow\text{Zn}$ bond between $[(\text{BDI})\text{Ga}]$ and $[(\text{tmeda})\text{ZnH}]^+$ fragments. Significant pyramidalization ($\Sigma_{(\text{N}-\text{Zn}-\text{Ga}, \text{N}-\text{Zn}-\text{N})} = 315^\circ$) of the zinc centre is consistent with the presence of a hydride ligand at one vertex of the distorted zinc-centred tetrahedron.

Layering a THF solution of **3** with *n*-pentane provided colourless single crystals of $[(\text{BDI})\text{Ga}(\text{H})\text{-}(\text{thf})\text{Zn}(\text{tmeda})][\text{BAR}_4^{\text{F}}]$ (**4**), which crystallises in the monoclinic space group $P2_1/n$. Compound **4** can be considered as the THF-adduct of **3a**, the gallium-bound hydride of which was located and freely refined. Coordination of THF to zinc results in only slight pyramidalization of the metal centre ($\Sigma_{(\text{N}-\text{Zn}-\text{Ga}, \text{N}-\text{Zn}-\text{N})} = 348^\circ$) and the $\text{Ga}-\text{Zn}$ bond is of similar length to **3a** (2.4030(5) Å vs. 2.3973(11) Å). The PMDTA derivative $[(\text{BDI})\text{Ga}(\text{H})\text{-Zn}(\text{pmdta})][\text{BAR}_4^{\text{F}}]$ (**5**; $\text{PMDTA} = \text{N},\text{N},\text{N}',\text{N}'',\text{N}'''$ -pentamethyldiethylenetriamine) was synthesised by an analogous procedure, and features a $\text{Ga}-\text{Zn}$ bond that is further elongated (2.4107(5) Å), presumably due to the stronger combined donor properties of the chelating triamine (see Supporting Information for details). A band at 1792 cm^{-1} in the solid state (KBr) FTIR spectrum of **3a** was assigned to the $\text{Ga}-\text{H}$ stretching mode. Consistent with increasing coordination number, the corresponding band appears at 1707 cm^{-1} for **4**, and 1692 cm^{-1} for **5**. The corresponding spectrum obtained for isolated samples of **3b** were reproducibly identical to that of **3a**. Given the observed preference for isomer **3a** in solution and by antisolvent crystallisation, we suspect that isomerisation may occur during sample preparation where lattice solvent is removed *in vacuo*.

The DFT calculated structures of **3a** and **3b** (B3PW91) are in good agreement to the X-ray crystal structures, but optimized bond lengths were slightly overestimated compared to the experimental data. A dative $\text{Ga}\rightarrow\text{Zn}$ bond of 86% *s*-character and 66% gallium contribution is consistent with **3b** as a donor-acceptor complex. As a result, the four-coordinate zinc centre carries a natural charge of 0.39,

whereas the gallium centre is more highly charged (1.22). Isomer **3a** involves a covalent Ga–Zn bond of 63% *p*-character with a 52% contribution from gallium and similar natural charges on each metal (0.73, Ga; 0.77, Zn). In both compounds, the HOMO involves the metal-metal and metal-hydride bonding orbitals (Figure 2). Whereas the LUMO of **3b** is delocalised over the BDI-ligand backbone, it is of π -symmetry and predominantly zinc-centred in **3a**. Compound **4** displays slight polarisation of the metal-metal bond towards gallium and predominantly BDI-based frontier molecular orbitals. In each of these compounds, the Ga–Zn Wiberg Bond Index (WBI) is consistent with a covalent single bond (0.87, **3a**; 0.84, **3b**; 0.86, **4**).

The NMR spectra of precipitated compound **3** are identical to that of recrystallised **3a**, **3b**, and **4**. In THF- d_8 , a single species with well-defined BDI and TMEDA resonances was observed and assigned to THF-adduct **4**, in rapid dissociative equilibrium with the solvent. A broadened resonance at $\delta_{\text{H}}=5.72$ ppm in the ^1H NMR spectrum was assigned to the gallium hydride, which shows intramolecular correlation peaks with the isopropyl groups of the nearby BDI ligand, but not to zinc-bound TMEDA in the corresponding ^1H - ^1H NOESY spectrum. The GaH chemical shift is comparable to that of **5** ($\delta_{\text{H}}=5.77$ ppm) and [(BDI)Ga(H)–(H)Al(tmeda)][B(3,5-Me₂-C₆H₃)₄] ($\delta_{\text{H}}=5.39$ ppm in C₆D₅Br).^[18a] When dissolved in fluorobenzene/C₆D₆ (10:1), full dissociation of THF from compound **4** was indicated in the ^1H NMR spectrum, which is otherwise identical to that of **3a** and **3b**. In this solvent, the major species was assigned to the gallium-hydride isomer **3a**, which shows well defined ligand signals and a broad GaH resonance at $\delta_{\text{H}}=5.75$ ppm. In addition to intramolecular coupling with the nearby isopropyl groups, ^1H - ^1H NOESY experiments show intermolecular exchange of the hydride with a broad signal centred at $\delta_{\text{H}}=4.16$ ppm, tentatively assigned to the ZnH environment of isomer **3b**. Broadened BDI signals of **3b**

were tentatively assigned on the basis of intermolecular correlation to the corresponding resonances associated with the ligand of **3a**. These observations hint at a dynamic equilibrium between the two isomers, and computational assessment at the DFT level (B3PW91) agrees with a slight thermodynamic preference for **3a** ($\Delta H_{\text{PhF}}=0.0$ kcal mol⁻¹) over **3b** ($\Delta H_{\text{PhF}}=3.3$ kcal mol⁻¹) in fluorobenzene solution. Isomerisation by hydride transfer proceeds via the 3-membered transition state **TS1** ($\Delta H_{\text{PhF}}^{\ddagger}=18.0$ kcal mol⁻¹). Attempts to experimentally determine an equilibrium constant by variable temperature (V.T.) NMR experiments in fluorobenzene solution were frustrated by the low abundance and substantial line-broadening of the minor species. Although dissociation of THF from **4** was calculated to be endothermic, it is entropically favourable in fluorobenzene (exergonic by $\Delta G_{\text{PhF}}=6.1$ kcal mol⁻¹; see Supporting Information, Scheme S11). Invoking a THF solvent model returned a similar potential energy surface, consistent with observation of a single species, **4** ($\Delta H_{\text{THF}}=-5.2$ kcal mol⁻¹, with respect to **3a**; Figure 3) by NMR spectroscopy in THF- d_8 .

In THF- d_8 solution, **4**^[22] reacts under an H₂ atmosphere (ca. 1.5 bar) at 70 °C to yield a 1:1 mixture of **1-H₂** and [(tmeda)ZnH(thf)][BAR₄^F] (**2b**)^[19a] in 75% spectroscopic yield over the course of 63 h, with net oxidative addition of H₂ across the Ga–Zn bond (Scheme 3). Repeating the reaction with D₂ resulted in an unresolved mixture of isotopomers. Dissociation of THF appears crucial to this reactivity, as coordinatively saturated PMDTA derivative **5** proved inert towards H₂ under these conditions. It was thus anticipated that a more rapid reaction would occur between H₂ and the THF-free complex **3** in fluorobenzene solution. By contrast, the ^1H NMR spectrum of this mixture remained unchanged after 20 h at 70 °C. Repeating this reaction with D₂ over the course of 3 days at 70 °C, however, resulted in formation of HD, consumption of the GaH resonance in the ^1H NMR spectrum and appearance of a GaD signal at $\delta_{\text{2H}}=5.73$ ppm in the ^2H NMR spectrum, indicating H/D exchange.^[23]

Speculating that isotopic exchange originated from microscopic reversibility of a hydrogenation-dehydrogenation equilibrium biased towards the dehydrogenated species, **1-H₂** and **2a** were dissolved in fluorobenzene/C₆D₆ and the solution investigated by V.T. ^1H NMR spectroscopy

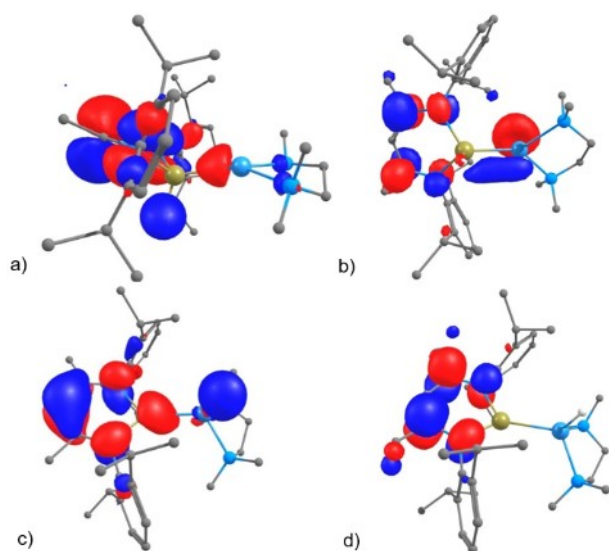
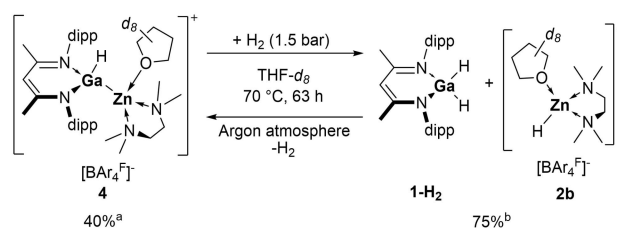
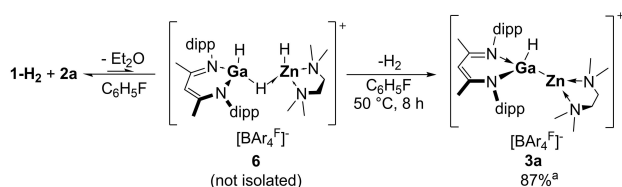


Figure 2. DFT (B3PW91) calculated HOMO (a,c) and LUMO (b,d) of compounds **3** (a,b) and **3'** (c,d).



Scheme 3. Reaction of compound **4** with H₂ and of **1-H₂** with **2b** in THF- d_8 . Reaction conditions in both cases: 70 °C, 63 h. Spectroscopic yields determined by integration of ^1H NMR spectrum: ^ayield obtained from dehydrogenation of **1-H₂** and **2b**; ^byield obtained from hydrogenation of **4**, both products formed in equimolar quantities.

under an argon atmosphere. The BDI ligand signals remained largely unaffected over a temperature range 233–317 K, but the gallium hydride resonance became progressively broadened and upfield shifted with increasing temperature ($\delta_{\text{H}}=4.94$ ppm, $\omega_{1/2}=70$ Hz, 298 K) and compared to pure **1-H₂** ($\delta_{\text{H}}=5.06$ ppm, $\omega_{1/2}=13$ Hz, 298 K). Exchange cross-peaks between the gallium hydride resonance and a second species at $\delta_{\text{H}}=3.72$ ppm were also observed in a NOESY experiment at 233 K. These observations are consistent with an interaction between the mononuclear species through formation of a transient $\mu\text{-H}$ bridged dinuclear trihydride cation $[(\text{BDI})\text{Ga}(\text{H})(\mu\text{-H})\text{Zn}(\text{H})\text{-(tmeda)}][\text{BAR}_4\text{F}^-]$ (**6**, Scheme 4). Attempts to crystallise such a species by layering the aforementioned solution with *n*-pentane, however, repeatedly provided single crystals of dehydrogenation product **3a**. Heating a fluorobenzene solution of **1-H₂** and **2a** to 50 °C resulted in 87 % conversion to **3** as a mixture of isomers **3a** and **3b** over the course of



Scheme 4. Dehydrogenation of **1-H₂** in fluorobenzene solution mediated by **2a**. ^a Products **3a** and **3b** exist as an equilibrium mixture in this solvent. Only the major species **3a** is shown for simplicity. Broadening of the signals assigned to **3b** prevents reliable quantification of spectroscopic yield, and the more accurately determined total conversion of **1-H₂** to **3** as a mixture of isomers is reported instead.

48 h with concomitant production of H₂ (Scheme 4), as determined by in situ ¹H NMR spectroscopy. THF-*d*₈ solutions of **1-H₂** and **2b** are stable under argon at room temperature, but slowly dehydrogenate at 70 °C to provide **4** in 40 % spectroscopic yield after 2 days (Scheme 3). Recharging this mixture with H₂ returned **1-H₂** and **2b** in 73 % spectroscopic yield after 3 days at 70 °C. Furthermore, mixtures of **1-H₂** and **2b** undergo H/D exchange at 70 °C under a D₂ atmosphere. H/D exchange was not observed for pure **1-H₂**, which is also stable with respect to dehydrogenation in the absence of **2a/b**. In contrast to literature reports, compound **1** is unreactive towards H₂ in our hands.^[15]

The reaction between **4** and H₂ was computationally explored at the DFT (B3PW91) level with THF solvent correction. Displacement of THF and addition of H₂ across the Ga–Zn bond of **4** faces a barrier of $\Delta H_{\text{THF}}^\ddagger=43.1$ kcal mol⁻¹ (see Supporting Information, Scheme S6). Prior dissociation of THF and hydride transfer to provide zinc-hydride isomer **3b** ($\Delta H_{\text{THF}}=9.0$ kcal mol⁻¹) is endothermic, but enables access to a less kinetically demanding pathway involving insertion H₂ into the Ga→Zn bond of **3b** via an FLP-like transition state **TS2** ($\Delta H_{\text{THF}}^\ddagger=39.3$ kcal mol⁻¹, Figure 3). Initial formation of dinuclear trihydride **6** is endothermic ($\Delta H_{\text{THF}}=7.3$ kcal mol⁻¹), but coordination of THF to the Lewis-acidic zinc cation drives the reaction towards hydrogenated products **1-H₂** and **2b** ($\Delta H_{\text{THF}}=-5.6$ kcal mol⁻¹). Direct oxidative addition of H₂ to compound **1** was calculated to be slightly exothermic ($\Delta H_{\text{THF}}=-8.0$ kcal mol⁻¹), but kinetically prohibitive ($\Delta H_{\text{THF}}^\ddagger=50.8$ kcal mol⁻¹; see Supporting Information, Scheme S3). Although the enthalpy of hydrogenation of **3a** ($\Delta H_{\text{pHF}}=12.3$ kcal mol⁻¹) to **6** ($\Delta H_{\text{pHF}}=14.2$ kcal mol⁻¹) was

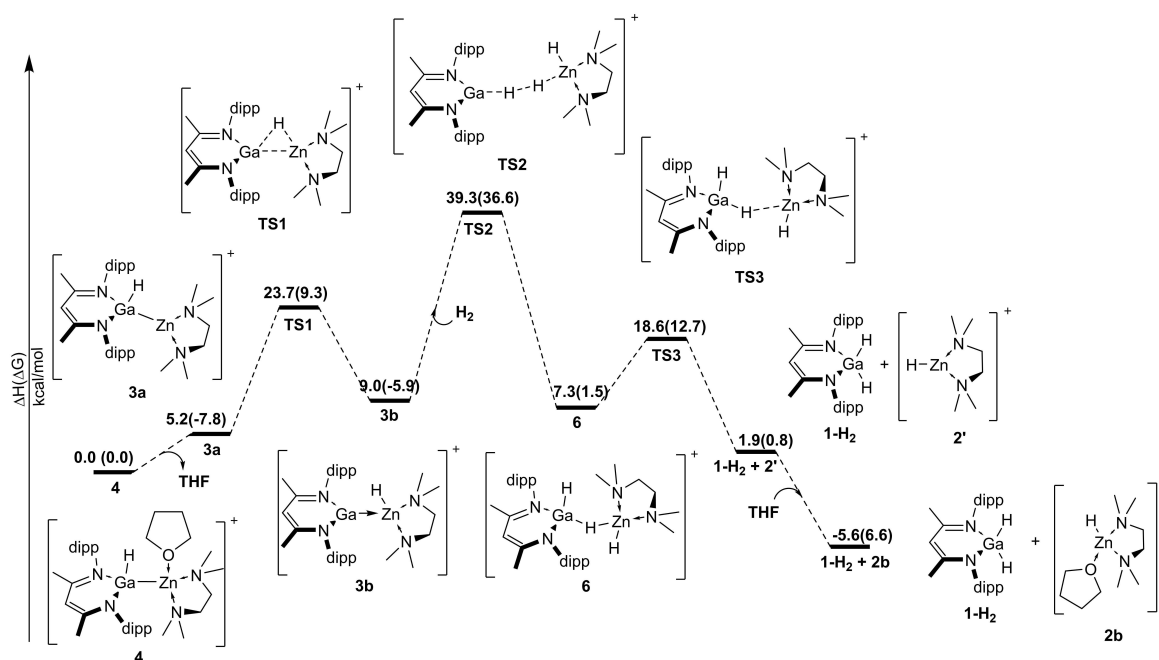


Figure 3. DFT calculated pathway for isomerisation of **3a** and **3b** and the reaction of **4** with H₂. Calculated potential energies ΔH_{THF} (kcal mol⁻¹) are shown with Gibbs free energies ΔG_{THF} (kcal mol⁻¹) in parentheses. Contributions from the $[\text{BAR}_4\text{F}^-]$ anion, THF solvent and dispersion interactions are included, see Supporting Information for details.

calculated to be near thermoneutral in fluorobenzene, it is entropically disfavoured and not observed, since the stable THF-adduct **2a** cannot form. The experimentally observed dehydrogenation of **1-H₂** and **2a** ($\Delta H_{\text{PhF}}=0.0 \text{ kcal mol}^{-1}$) to **3a** ($\Delta H_{\text{PhF}}=12.3 \text{ kcal mol}^{-1}$) via **6** and **TS2** ($\Delta H_{\text{PhF}}^{\ddagger}=45.4 \text{ kcal mol}^{-1}$) in fluorobenzene was calculated to be endothermic on account of the prerequisite dissociation of Et₂O from **2a** (see Supporting Information, Scheme S12). Thus, overall dehydrogenation may be rationalised by entropically favourable release of Et₂O and H₂. Although subject to intrinsically high errors due to the harmonic approximation, the overall dehydrogenation was calculated to be exergonic by $\Delta G_{\text{PhF}}=-7.0 \text{ kcal mol}^{-1}$ (see Supporting Information, Scheme S12). Similar arguments can be made for the slow partial dehydrogenation of **1-H₂** and **2b** to give **4** in THF ($\Delta G_{\text{THF}}=-6.6 \text{ kcal mol}^{-1}$, Figure 3).^[24] Dehydrogenation of **1-H₂** can be considered to be Lewis-acid mediated through formation of a μ_2 -H interaction between **1-H₂** and the *d*¹⁰ zinc cation, and is thus mechanistically distinct from previously reported TM-mediated processes.^[16,25]

In conclusion, dihydrogen adds across a Ga–Zn bond with formal two electron oxidation of the gallium(I) centre. Stabilisation of the Lewis acidic [(tmeda)ZnH]⁺ cation by coordinating THF is decisive in favouring H–H cleavage in this solvent, resulting in reversible formation of [(BDI)-GaH₂]. Conversely, in weakly coordinating fluorobenzene solution, the system is biased towards entropically driven dehydrogenation. These findings highlight the potential for heterobimetallics to optimise catalytically relevant oxidative addition and reductive elimination in main-group complexes.^[26]

Acknowledgements

We thank the Deutsche Forschungsgemeinschaft for financial support. We acknowledge R. Bomahrat and Dr. G. Fink for assisting with NMR experiments, Dr. T. P. Spaniol for advice regarding crystal structure refinement, and Prof. M. S. Hill (University of Bath) for helpful discussions. L.M. is a senior member of the Institut Universitaire de France and acknowledges the Alexander von Humboldt Foundation for financial support as well as CalMip for a generous grant of computing time. Open Access funding enabled and organized by Projekt DEAL.

Conflict of Interest

The authors declare no conflict of interest.

Data Availability Statement

The data that support the findings of this study are available in the supplementary material of this article.

Keywords: Dehydrogenation · Heterometallic Complexes · Hydrogenation · Main Group Compounds · Solvent Effects

- [1] a) I. Wender, H. W. Sternberg, M. Orchin, *J. Am. Chem. Soc.* **1953**, *75*, 3041–3042; b) F. Hebrard, P. Kalck, *Chem. Rev.* **2009**, *109*, 4272–4282.
- [2] T. Chu, G. I. Nikonov, *Chem. Rev.* **2018**, *118*, 3608–3680.
- [3] A. Hinz, A. Schulz, A. Villinger, *Angew. Chem. Int. Ed.* **2016**, *55*, 12214–12218; *Angew. Chem.* **2016**, *128*, 12402–12406.
- [4] a) E. von Grotthuss, S. E. Prey, M. Bolte, H. W. Lerner, M. Wagner, *J. Am. Chem. Soc.* **2019**, *141*, 6082–6091; b) E. von Grotthuss, M. Diefenbach, M. Bolte, H. W. Lerner, M. C. Holthausen, M. Wagner, *Angew. Chem. Int. Ed.* **2016**, *55*, 14067–14071; *Angew. Chem.* **2016**, *128*, 14273–14277.
- [5] S. Wang, T. J. Sherbow, L. A. Berben, P. P. Power, *J. Am. Chem. Soc.* **2018**, *140*, 590–593.
- [6] R. C. Turnell-Ritson, J. S. Sapsford, R. T. Cooper, S. S. Lee, T. Foldes, P. A. Hunt, I. Papai, A. E. Ashley, *Chem. Sci.* **2018**, *9*, 8716–8722.
- [7] a) J. Lam, K. M. Szkop, E. Mosafieri, D. W. Stephan, *Chem. Soc. Rev.* **2019**, *48*, 3592–3612; b) D. W. Stephan, *Science* **2016**, *354*, aaf7229; c) G. Ménard, D. W. Stephan, *Angew. Chem. Int. Ed.* **2012**, *51*, 8272–8275; *Angew. Chem.* **2012**, *124*, 8397–8400; d) D. J. Scott, M. J. Fuchter, A. E. Ashley, *Chem. Soc. Rev.* **2017**, *46*, 5689–5700.
- [8] B. Ginovska, T. Autrey, K. Parab, M. E. Bowden, R. G. Potter, D. M. Camaioni, *Chem. Eur. J.* **2015**, *21*, 15713–15719.
- [9] a) A. Datta, *J. Phys. Chem. C* **2008**, *112*, 18727–18729; b) S. J. Bonyhady, C. Jones, S. Nembenna, A. Stasch, A. J. Edwards, G. J. McIntyre, *Chem. Eur. J.* **2010**, *16*, 938–955; c) S. P. Green, C. Jones, A. Stasch, *Science* **2007**, *318*, 1754–1757.
- [10] N. Tsukahara, H. Asakawa, K. H. Lee, Z. Lin, M. Yamashita, *J. Am. Chem. Soc.* **2017**, *139*, 2593–2596.
- [11] R. M. Charles, T. P. Brewster, *Coord. Chem. Rev.* **2021**, *433*, 213765.
- [12] a) A. Friedrich, J. Eyslein, J. Langer, C. Farber, S. Harder, *Angew. Chem. Int. Ed.* **2021**, *60*, 16492–16499; *Angew. Chem.* **2021**, *133*, 16628–16635; b) S. Brand, H. Elsen, J. Langer, S. Grams, S. Harder, *Angew. Chem. Int. Ed.* **2019**, *58*, 15496–15503; *Angew. Chem.* **2019**, *131*, 15642–15649; c) S. Brand, H. Elsen, J. Langer, W. A. Donaubaauer, F. Hampel, S. Harder, *Angew. Chem. Int. Ed.* **2018**, *57*, 14169–14173; *Angew. Chem.* **2018**, *130*, 14365–14369; d) C. Bakewell, B. J. Ward, A. J. P. White, M. R. Crimmin, *Chem. Sci.* **2018**, *9*, 2348–2356.
- [13] a) S. Aldridge, A. J. Downs, *The Group 13 Metals Aluminium, Gallium, Indium and Thallium: Chemical Patterns and Peculiarities*, 1st ed., Wiley, Chichester, **2011**; b) C. Dohmeier, D. Loos, H. Schnöckel, *Angew. Chem. Int. Ed. Engl.* **1996**, *35*, 129–149; *Angew. Chem.* **1996**, *108*, 141–161; c) J. C. Beamish, A. Boardman, I. J. Worrall, *Polyhedron* **1991**, *10*, 95–99; d) K. L. Brown, D. Hall, *J. Chem. Soc. Dalton Trans.* **1973**, 1843–1845; e) A. Barthélemy, K. Glootz, H. Scherer, A. Hanske, I. Krossing, *Chem. Sci.* **2022**, *13*, 439–453; f) P. Dabringhaus, A. Barthélemy, I. Krossing, *Z. Anorg. Allg. Chem.* **2021**, *647*, 1660–1673; g) M. Schorpp, R. Tamim, I. Krossing, *Dalton Trans.* **2021**, *50*, 15103–15110; h) J. M. Slattery, A. Higelin, T. Bayer, I. Krossing, *Angew. Chem. Int. Ed.* **2010**, *49*, 3228–3231; *Angew. Chem.* **2010**, *122*, 3297–3301.
- [14] a) C. A. Caputo, J. Koivistoinen, J. Moilanen, J. N. Boynton, H. M. Tuononen, P. P. Power, *J. Am. Chem. Soc.* **2013**, *135*, 1952–1960; b) Z. L. Zhu, X. P. Wang, Y. Peng, H. Lei, J. C. Fettinger, E. Rivard, P. P. Power, *Angew. Chem. Int. Ed.* **2009**, *48*, 2031–2034; *Angew. Chem.* **2009**, *121*, 2065–2068.
- [15] a) A. Seifert, D. Scheid, G. Linti, T. Zessin, *Chem. Eur. J.* **2009**, *15*, 12114–12120; b) Contrary to the results reported in reference 15a, compound **1** is unreactive towards H₂ (ca.

- 1.5 bar) at room temperature or over the course of 1 week at 70 °C in our hands (see Supporting Information for details; see also reference 18b).
- [16] a) A. Caise, J. A. B. Abdalla, R. Tirfoin, A. J. Edwards, S. Aldridge, *Chem. Eur. J.* **2017**, *23*, 16906–16913; b) J. Turner, J. A. B. Abdalla, J. I. Bates, R. Tirfoin, M. J. Kelly, N. Phillips, S. Aldridge, *Chem. Sci.* **2013**, *4*, 4245–4250.
- [17] a) R. J. Wehmschulte, R. Peverati, D. R. Powell, *Inorg. Chem.* **2019**, *58*, 12441–12445; b) L. J. Morris, P. Ghana, T. Rajeshkumar, A. Carpentier, L. Maron, J. Okuda, *Angew. Chem. Int. Ed.* **2022**, *61*, e202114629; *Angew. Chem.* **2022**, *134*, e202114629.
- [18] a) L. J. Morris, A. Carpentier, L. Maron, J. Okuda, *Chem. Commun.* **2021**, *57*, 9454–9457; b) L. J. Morris, T. Rajeshkumar, L. Maron, J. Okuda, *Chem. Eur. J.* **2022**, *28*, e202201480.
- [19] a) F. Ritter, T. P. Spaniol, I. Douair, L. Maron, J. Okuda, *Angew. Chem. Int. Ed.* **2020**, *59*, 23335–23342; *Angew. Chem.* **2020**, *132*, 23535–23543; b) See Supporting Information for full details on compound **2a**.
- [20] a) I. L. Fedushkin, A. N. Lukoyanov, A. N. Tishkina, M. O. Maslov, S. Y. Ketkov, M. Hummert, *Organometallics* **2011**, *30*, 3628–3636; b) I. L. Fedushkin, A. N. Lukoyanov, S. Y. Ketkov, M. Hummert, H. Schumann, *Chem. Eur. J.* **2007**, *13*, 7050–7056; c) O. Bonello, C. Jones, A. Stasch, W. D. Woodul, *Organometallics* **2010**, *29*, 4914–4922; d) C. Jones, R. P. Rose, A. Stasch, *Dalton Trans.* **2007**, 2997–2999; e) A. Kempfer, C. Gemel, R. A. Fischer, *Inorg. Chem.* **2008**, *47*, 7279–7285; f) A. Kempfer, C. Gemel, T. Cadenbach, R. A. Fischer, *Inorg. Chem.* **2007**, *46*, 9481–9487.
- [21] K. Freitag, H. Banh, C. Gemel, P. Jerabek, R. W. Seidel, G. Frenking, R. A. Fischer, *Inorg. Chem.* **2015**, *54*, 352–358.
- [22] An isolated sample of compound **3** was dissolved in THF-*d*₈ to provide a solution of **4**.
- [23] H/D exchange was also observed at the γ -position of the BDI ligand backbone, see Supporting Information for details.
- [24] a) M. J. Bezdek, S. Guo, P. J. Chirik, *Science* **2016**, *354*, 730–733; b) J. J. Warren, T. A. Tronic, J. M. Mayer, *Chem. Rev.* **2010**, *110*, 6961–7001.
- [25] M. J. Butler, M. R. Crimmin, *Chem. Commun.* **2017**, *53*, 1348–1365.
- [26] Deposition Numbers 2153944, 2153945, 2153946, 2153947 and 2153948 contain the supplementary crystallographic data for this paper. These data are provided free of charge by the joint Cambridge Crystallographic Data Centre and Fachinformationszentrum Karlsruhe Access Structures service.

Manuscript received: June 21, 2022

Accepted manuscript online: July 14, 2022

Version of record online: August 4, 2022